CHAPTER IV

RESULTS AND DISCUSSION

In this research, Si-SBA-15 and modified acid catalysts Al-SBA-15 were synthesized, characterized and investigated in cracking process of waste from biodiesel production. In addition, the biodiesel waste was determined the composition.

4.1 The physico-chemical properties of SBA-15

4.1.1 XRD results of pure silica SBA-15

The small-angle XRD patterns of as-synthesized and calcined mesoporous Si-SBA-15 are shown in Figure 4.1. Both samples are shown the typical pattern of hexagonal structure [23], as-synthesized SBA-15 exhibits the peak positions located at two-theta of 0.8°, 1.5° and 1.7° for plane (100), (110) and (200) respectively. After remove the template, the calcined sample performs higher intensity at all reflections than as-synthesized sample because the structure directing agent in pores is completely removed. In addition, the XRD pattern of the calcined sample is slightly shifted to the larger angle because the unit cell shrinks after sample is heated at high temperature (about 550°C) [63].

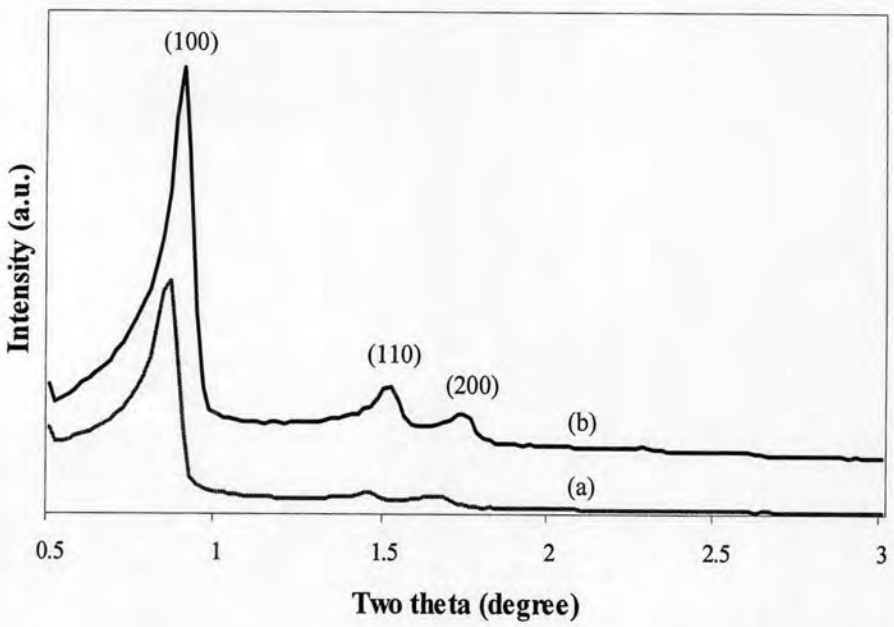

Figure 4.1 XRD patterns of (a) as-synthesized Si-SBA-15, (b) calcined Si-SBA-15.

4.1.2 Sorption properties of SBA-15

The N_2 adsorption-desorption isotherm and pore size distribution of calcined Si-SBA-15 are shown in Figure 4.2. This sample performed isotherm type IV of IUPAC classification and exhibited a hysteresis loop H1-type which was characteristic of large-pore mesoporous materials with narrow pore size distribution [64] with the pore diameter of 9.23 nm using Barrett-Joiner-Halenda (BJH) method. The total specific surface areas of pure SBA-15 was calculated using Brunauer, Emmett and Teller (BET) equation, which was found at 862 m^2/g.

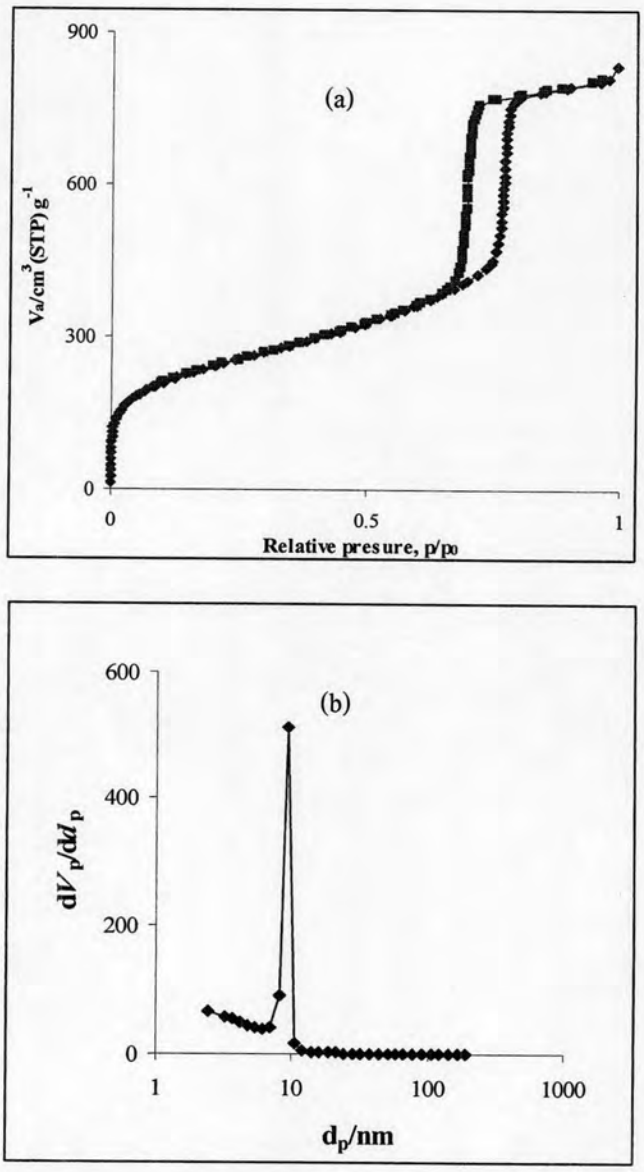

Figure 4.2 (a) N_2 adsorption-desorption isotherm and (b) BJH-pore size distribution of calcined SBA-15.

4.1.3 SEM images of SBA-15

The SEM images of calcined SBA-15 sample at different magnifications are shown in Figure 4.3. Pure silica SBA-15 performs regular dispersion containing small rod particles about 0.9 × 1.2 μm which agglomerated to rope-liked structure.

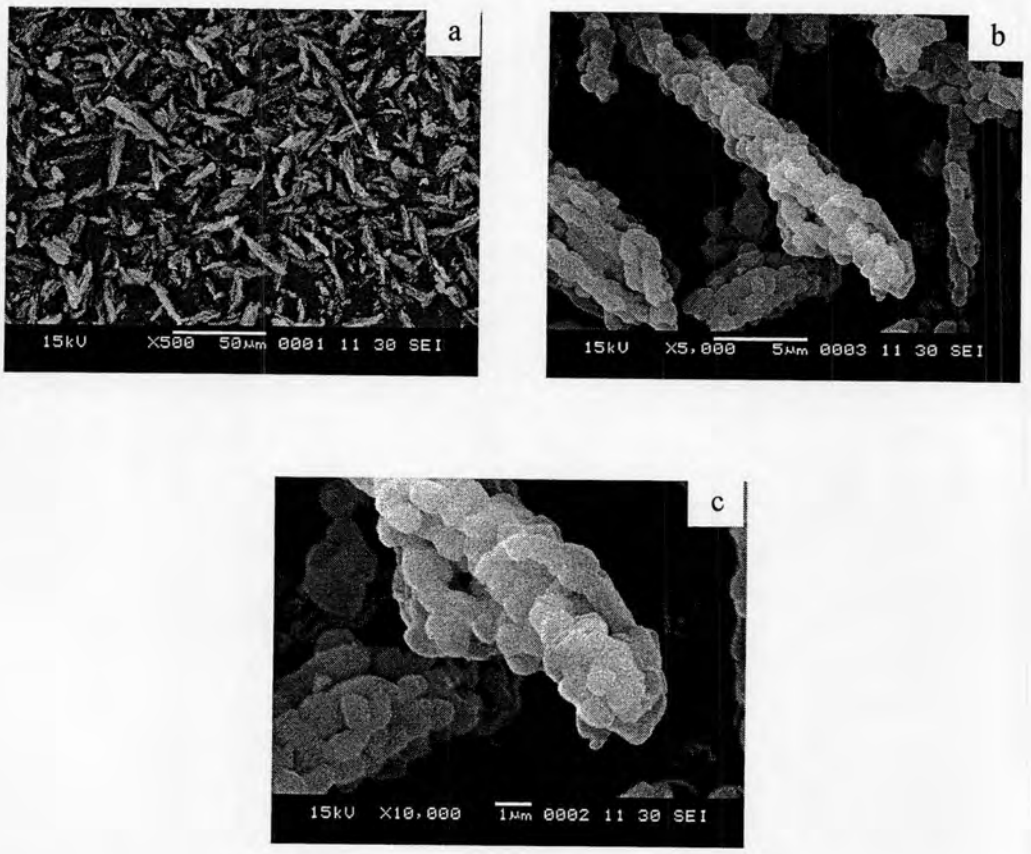

Figure 4.3 The SEM images of calcined pure SBA-15 at different magnifications (a) ×500, (b) ×5,000, and (c) ×10,000.

4.2 The physico-chemical properties of Al-SBA-15

4.2.1 XRD results

In this research, Al-SBA-15 were synthesized with Si/Al ratios in gel composition of 10, 25, 50, 100, and 200 by alumination method following Kevan *et al.* [24]. The value inside the parenthesis is the value for Si/Al ratio in reactant mixture. The XRD patterns of Al-SBA-15 at various Si/Al ratios compared to calcined Si-SBA-15 are shown in Figure 4.4. All XRD results indicate that the catalysts retain the ordered structure of SBA-15 during the post synthesis process. The peaks of various Si/Al ratios in Al-SBA-15 exhibited increasing intensity of the (100) reflection plane along with decreasing aluminum contents. Additionally, XRD patterns of the modified materials were shifted slightly to higher angle comparing to Si-SBA-15 resulting from the shrinkage during the recalcination process [65].

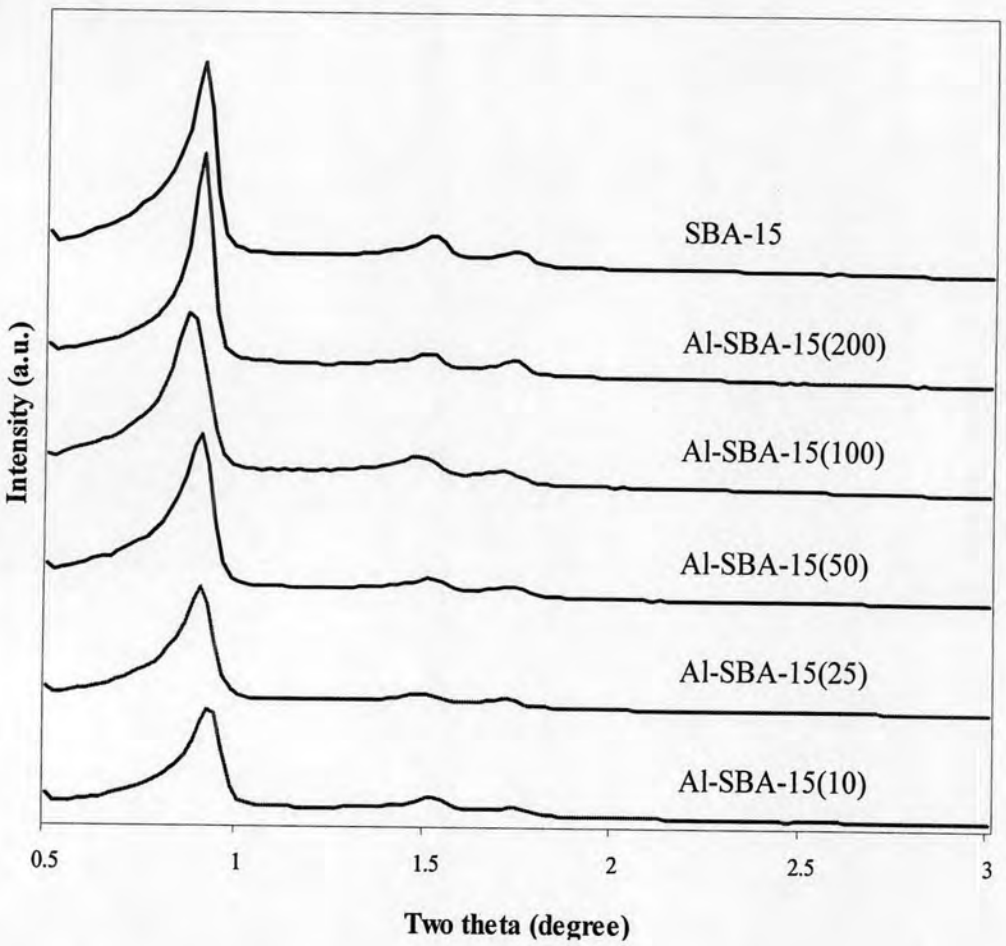

Figure 4.4 XRD patterns of calcined or dried Al-SBA-15 with various Si/Al mole ratios in reactant mixture.

4.2.2 Sorption properties of Al-SBA-15

The N_2 adsorption-desorption isotherm of alumination of SBA-15 catalysts in various Si/Al mole ratios are shown in Figure 4.5. Although, modified materials are inserted Al ion in the framework, the isotherms are classified in type IV, similar to the pure SBA-15. Textural properties of calcined catalysts are shown in Table 4.1.

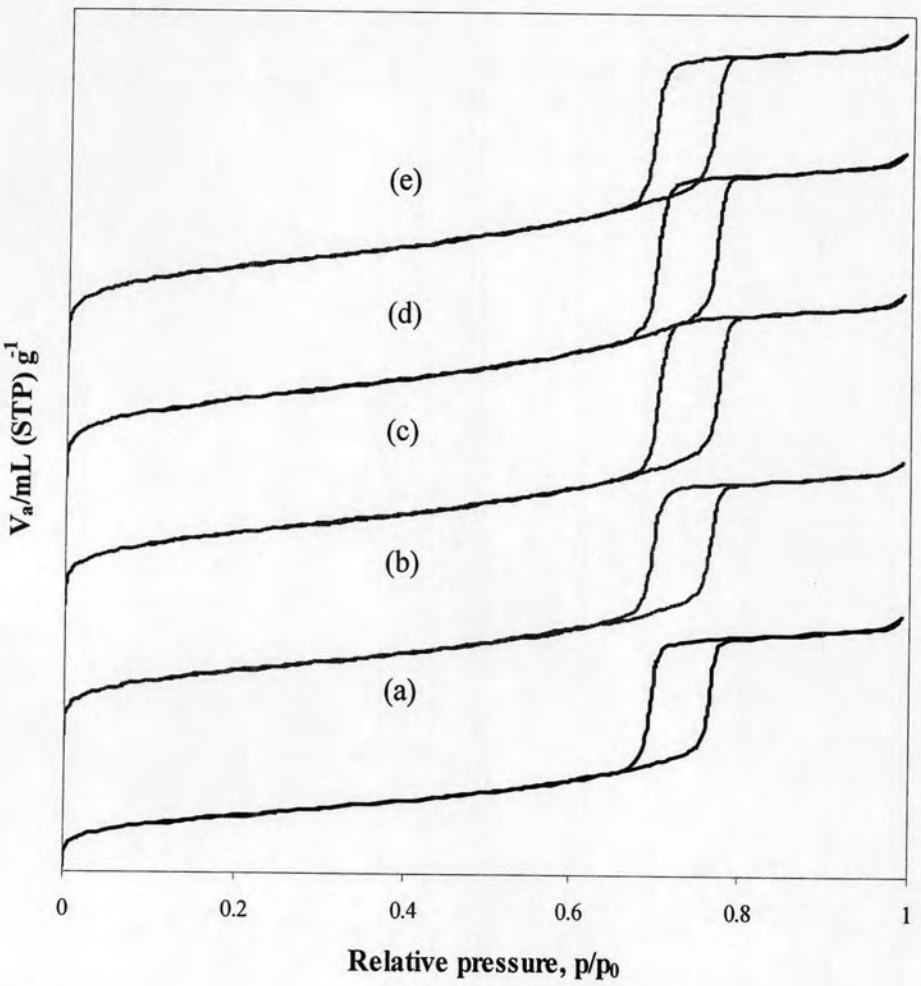

Figure 4.5 N_2 adsorption-desorption isotherms of (a) Al-SBA-15(10), (b) Al-SBA-15(25), (c) Al-SBA-15(50), (d) Al-SBA-15(100), and (e) Al-SBA-15(200).

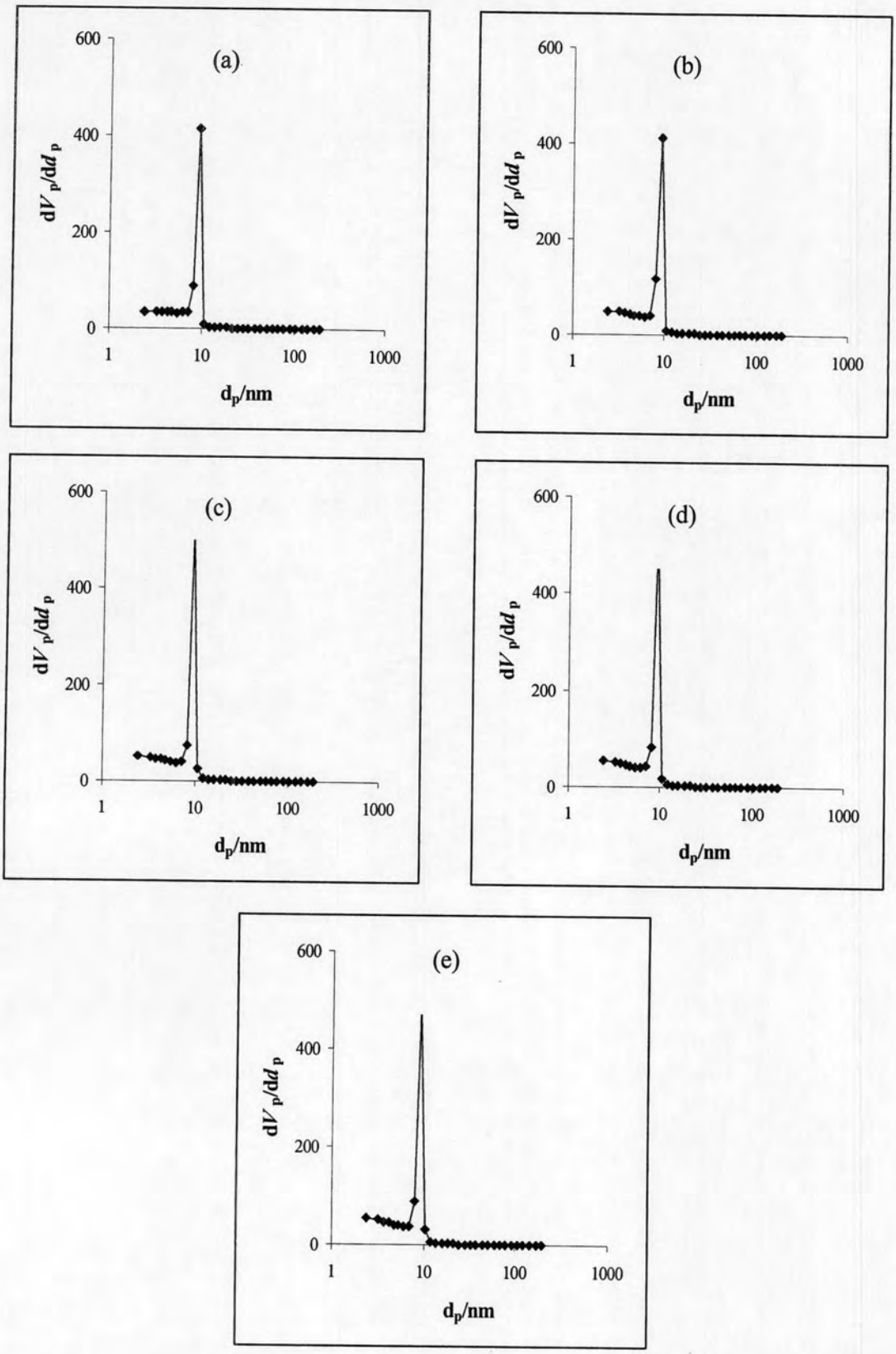

Figure 4.6 BJH-Pore size distributions of (a) Al-SBA-15(10), (b) Al-SBA-15(25), (c) Al-SBA-15(50), (d) Al-SBA-15(100), and (e) Al-SBA-15(200).

The pore size distribution obtained from BJH equation is shown in Figure 4.6. All sample exhibit a narrow distribution with the pore size of 9.23 nm. By comparing to the pore size of pure silica SBA-15 in Figure 4.2(b), the pore size of all Al-SBA-15 samples still remained unchanged, indicating the extreme stability of Al-SBA-15.

Table 4.1 Textural properties of calcined SBA-15 and Al-SBA-15 with various Si/Al ratios

Sample	Total specific surface area[a] ($m^2 \cdot g^{-1}$)	Pore size distribution[b] (nm)	Mesopore volume[b] ($cm^3 \cdot g^{-1}$)	$d_{(100)}$[c] (nm)	Wall thickness[d] (nm)
Si-SBA-15	862	9.23	1.154	9.98	2.29
Al-SBA-15(200)	722	9.23	1.100	9.58	1.83
Al-SBA-15(100)	703	9.23	1.132	9.56	1.81
Al-SBA-15(50)	645	9.23	1.103	9.51	1.75
Al-SBA-15(25)	587	9.23	0.996	9.42	1.65
Al-SBA-15(10)	469	9.23	0.900	9.31	1.52

[a]Calculated using the BET plot method,

[b]Calculated using the BJH method,

[c]Calculated using XRD, Jade5.6,

[d]Calculated as: a_0-pore size ($a_0 = 2 \times d_{(100)} / \sqrt{3}$).

Incorporated Al in the SBA-15 framework leads to a reduction in the amount of nitrogen up taken in SBA-15 depending on the quantities of aluminum due to the decreasing of mesoporous volume. This result is in agreement with those in literatures [35-36, 66]. In addition, when Al content was increased, the d-spacing was decreased indicating that the distance from each plane was reduced. Considering the effect of aluminum content in catalysts, wall thickness was calculated in the same method as Stucky *et al.* [23]. The data showed that the wall thickness decreased when aluminum quantity increased, corresponding to the decrease of d-spacing as $d_{(100)}$ in the equation. However, for low aluminum content such as Si/Al = 100 and 200 the wall thickness dose not significantly change.

4.2.3 SEM images of Al-SBA-15

The SEM images of modified acid SBA-15 samples are illustrated in Figure 4.7. All various Si/Al ratio samples show small rod particles. From aluminum

additions, the small rod particles are eliminated from the rope-like agglomeration. At Si/Al = 10, it performs many rod particle that breaks out of the aggregation, whereas at higher Si/Al ratios (25-200) the eliminated particle found less, and absent for pure SBA-15 as showed in Figure 4.3. However the rod shape of individual particle remains the same.

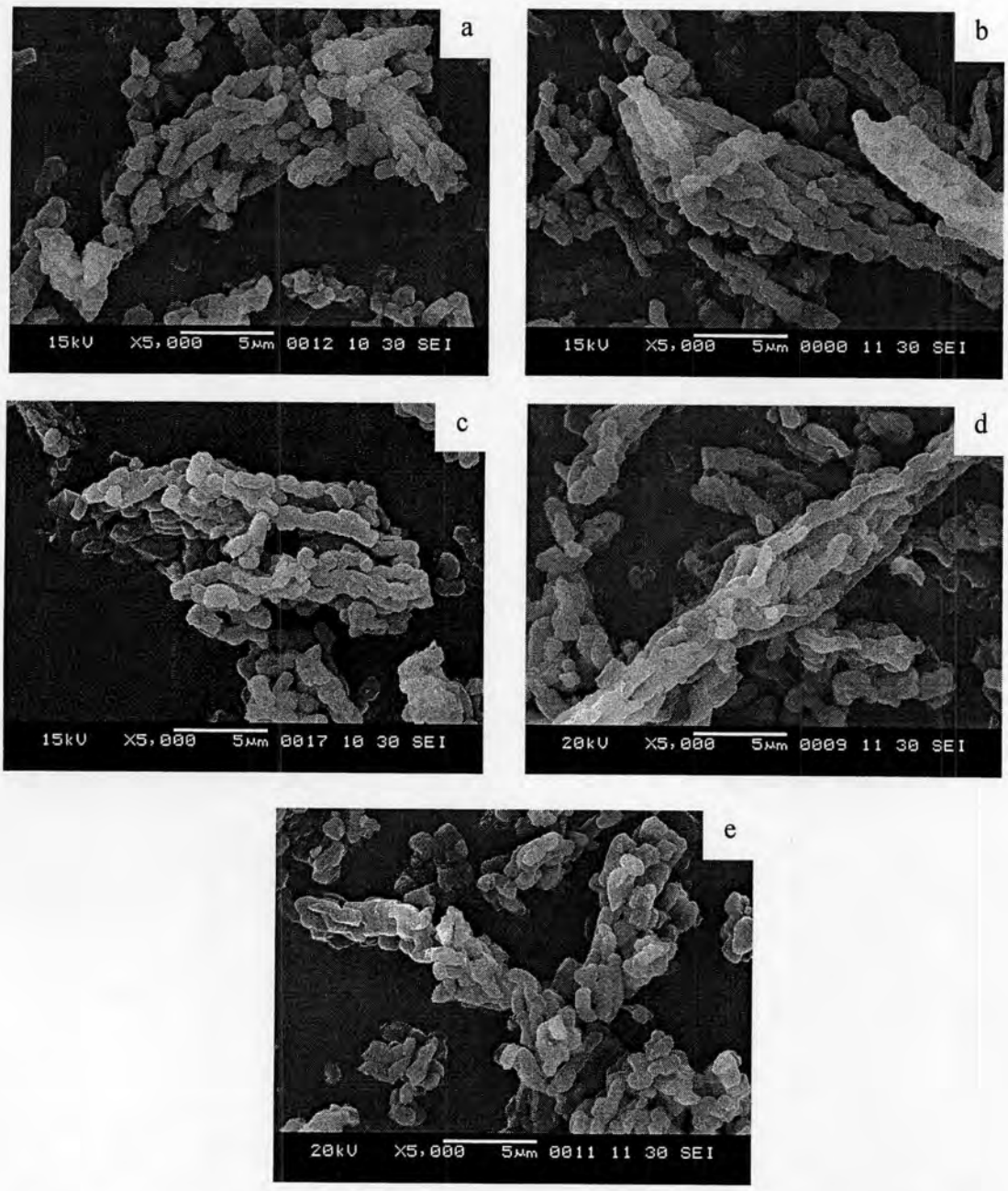

Figure 4.7 SEM images of (a) Al-SBA-15(10), (b) Al-SBA-15(25),(c) Al-SBA-15(50), (d) Al-SBA-15(100), and (e) Al-SBA-15(200).

4.2.4 Elemental analysis

The Si/Al ratios by mole in gel and in product of the Al-SBA-15 materials are compared in Table 4.2. The elemental analysis result suggests that the parts of aluminum are in the structure of catalyst. The Si/Al molar ratios in the reactant mixture for Al-SBA-15 synthesized by post synthesis are less than found in catalysts. In some causes the structural framework of pure silica SBA-15 was collapsed, thus the silica in the framework was a smaller amount. The content of the alumina (Al_2O_3) in sodium aluminate as aluminum source was higher quantity than calculation.

However, data from only ICP-AES technique cannot exhibit the position of aluminum atom, whether it located in framework or extra-framework, therefore data from ^{27}Al-NMR is needed for identification.

Table 4.2 Si/Al ratios in gel composition and in product of Al-SBA-15 catalysts

Sample	Si/Al mole ratios	
	in gel composition[a]	in catalysts[b]
Al-SBA-15(10) (H^+ form)	10	7.95
Al-SBA-15(25) (H^+ form)	25	18.5
Al-SBA-15(50) (H^+ form)	50	33.36
Al-SBA-15(100) (H^+ form)	100	69.30
Al-SBA-15(200) (H^+ form)	200	130.06

[a]Calculated from reagent quantities,

[b]Alumimum (Al) was determined by ICP-AES and sodium (Na) was determined by AAS.

4.2.5 ^{27}Al-MAS-NMR spectra

Solid state ^{27}Al-MAS-NMR can identify the form of aluminum atoms that are located in tetrahedral form (at the framework) or found in octahedral form (non-framework). ^{27}Al-MAS-NMR spectra of all modified acid catalysts are presented in Figure 4.8.

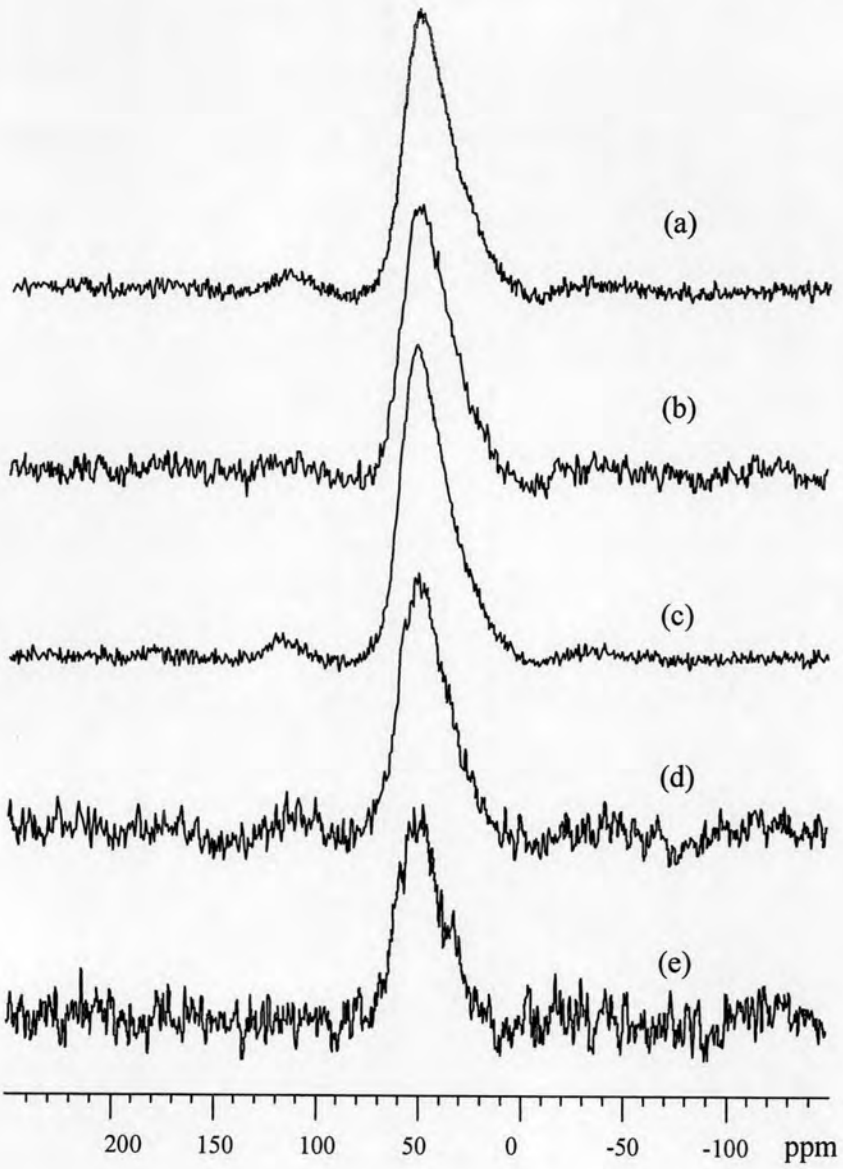

Figure 4.8 The ^{27}Al-MAS-NMR spectra of (a) Al-SBA-15(10), (b) Al-SBA-15(25), (c) Al-SBA-15(50), (d) Al-SBA-15(100), and (e) Al-SBA-15(200).

From ^{27}Al-MAS-NMR spectra, all Al-SBA-15 samples exhibit only one intense signal of the framework site at 55 ppm. indicating that the Al atoms are incorporated into the SBA-15 at purely tetrahedral framework position. In contrast to other reports [67-69] that ^{27}Al-MAS-NMR spectra of post-synthesized Al-SBA-15 samples exhibited octahedral aluminum. It is obvious that Al-SBA-15 with high aluminum amount (Si/Al =10-50) was illustrated more intense than low aluminum amount (Si/Al = 100-200) because of the quantity of Al atoms.

4.2.6 Acidity of the catalysts

Normally, ammonia TPD is utilized for determining the acidity of synthesis materials both acid site and the acid strength. However, the Al atoms quantity from the elemental analysis and the aluminum species from ^{27}Al MAS NMR can be estimated the acid site amount of Al-SBA-15 in Table 4.3.

Table 4.3 The quantity of acidic sites of Al-SBA-15 with various Si/Al ratios

Sample	Si/Al mole ratios in catalysts[a]	The number of acidic sites (arbitrary unit/g)
Al-SBA-15(10) (H^+ form)	7.95	0.1079
Al-SBA-15(25) (H^+ form)	18.5	0.0494
Al-SBA-15(50) (H^+ form)	33.36	0.0280
Al-SBA-15(100) (H^+ form)	69.30	0.0137
Al-SBA-15(200) (H^+ form)	130.06	0.0073

The acid sites quantities of Al-SBA-15 with various Si/Al ratios were increased following the aluminum contents. It concluded that the acidity was decreased by reducing Al content.

4.3 Determination of composition in waste from biodiesel production (WBP)

The compositions of waste from biodiesel production were determined to predict the mechanism or the product in cracking process. The make-up of the starting materials consist of glycerol content, ash, water content, and matter organic non-glycerol (MONG) as shown in Table 4.4. In addition, some properties such as the density and the pH value were investigated.

Table 4.4 The composition and physical properties of pure glycerol and WBP sample

Source	Composition of pure glycerol and WBP sample (%by mass)				Density at 20°C (g/mL)	pH
	Glycerol	Ash	Water	MONG		
Pure glycerol	98.16	0.13	N/A	$\leq$1.71	1.26	5.17
Biodiesel waste	37.18	6.49	1.85	54.48	1.03	10.47

Determination of glycerol content follows BS 5711: Part 3: 1979 [57] using oxidation reaction between glycerol and sodium periodate ($NaIO_4$) (Figure 4.9) to produce formaldehyde and formic acid. The amount of acid is used to estimate the glycerol quantity by titration with 0.125M standardized NaOH. The value of glycerol content in pure glycerol was 98.16% by mass which correlated to 99.00% by mass from the label of product, whereas WBP sample consists of 37.18% by mass of glycerol.

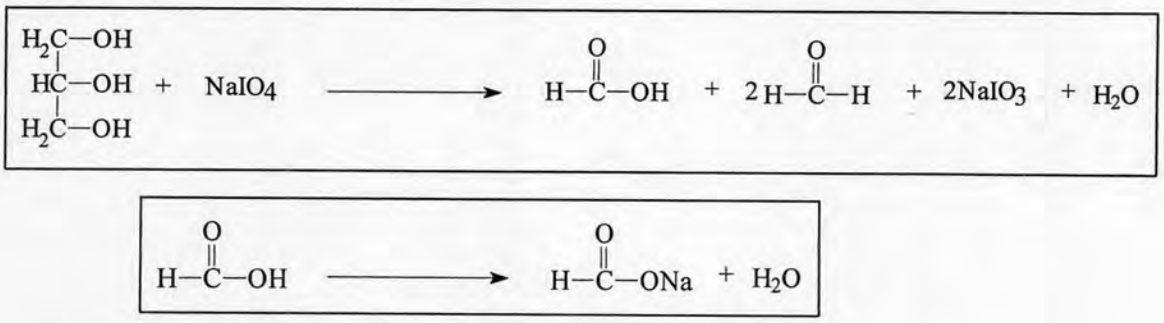

Figure 4.9 Reactions for determination of the glycerol content.

For ash content following BS 5711: Part 6: 1979[58], WBP sample gave the greater ash content than pure glycerol about 50 times. After calcination, WBP ash performed a brittle pale yellow thin network-pellet (Figure 4.10), while pure glycerol ash found nothing. This ash might be the inorganic impurity that cannot remove after calcined at 750°C.

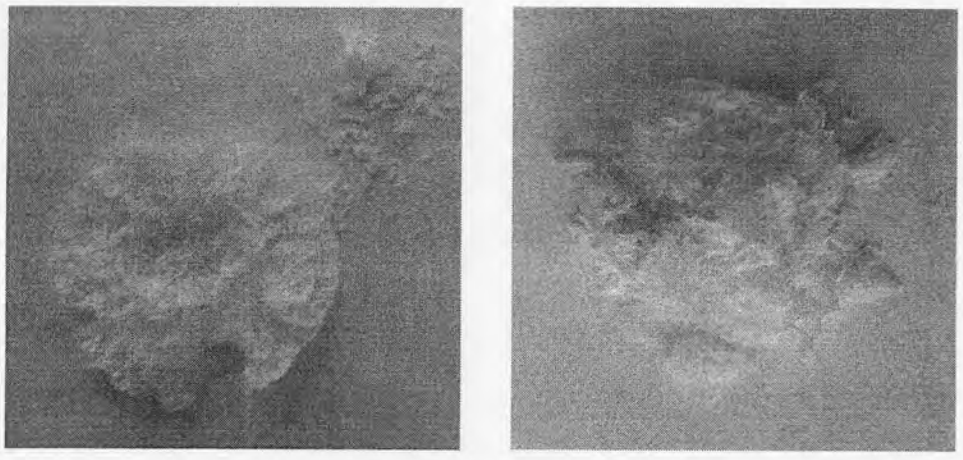

Figure 4.10 The images of waste from biodiesel production after calcined at 750°C.

Generally, water content can be determined by the Karl-Fischer method for calculating %MONG following BS 5711: Part 9: 1979 [58]. However, in this research, azeotropic distillation method D890-98(2003) [59] was utilized because the conventional method cannot detect the end-point in titration of base-starting material. In this method, moisture is removed from the sample by distillation as an azeotrope with toluene. The water is collected in a suitable trap (Dean-Stark trap). The amount of water in pure glycerol was not much enough for measurement, while 1.85% by mass of the moisture in WBP sample was observed.

The percentage by mass of Matter Organic Non-Glycerol (MONG) can be calculated by subtracting the summation of the quantity of glycerol, ash and water from 100 (as equation in Section 3.6.4) which modified from BS 5711: Part 9: 1979 [60]. In spite of the %MONG of pure glycerol was found only 1.71% by mass, the %MONG of WBP was 54.48% by mass as the major composition. Casanave *et al.* discussed that the MONG consists of methyl ester [70], which this cause MONG could be mono-, di- glyceride and methyl ester.

Both density at 20°C and the pH value of starting material were observed following BS 5711: Part 4 (1979) [61] and Part 5 (1979) [62], respectively. The density at 20°C of pure glycerol and WBP using pyknometer were 1.26 and 1.03 g/mL, respectively. The alkalinity or acidity of the samples was determined using Metrohm 744 equipped with glass electrode (modified from BS 5711: Part5: 1979). The pH of pure glycerol was 5.17 (weak acid starting material), while the alkalinity of WBP was 10.47 (basic starting material) which effects to the stability of catalysts.

4.4 Catalytic testing in biodiesel waste cracking

4.4.1 Effect of Si/Al ratios in the catalyst

The accumulative volumes of liquid fraction in the graduated cylinder obtained by thermal cracking and catalytic cracking of biodiesel waste at 400°C are shown in Figure 4.11. This plot accounts for the kinetic rate of cracking reaction. From the experimental, the kinetic rate of biodiesel waste pyrolysis is slower than catalytic cracking both in acidic catalysts and non-acidic catalyst. However, the overall rate of liquid fraction formation does not different from each catalyst.

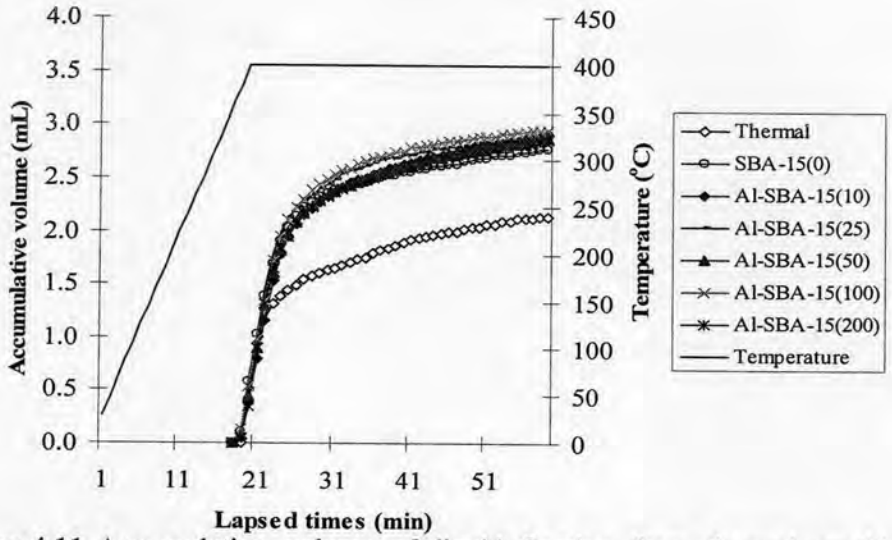

Figure 4.11 Accumulative volume of liquid fraction from thermal cracking and catalytic cracking of WBP over Al-SBA-15 samples with various Si/Al ratios at 400°C (Condition: 10%wt catalyst of substrate, N_2 flow of 20 mL/min and reaction time of 40 min).

The conversion value and product yield obtained by biodiesel waste cracking over thermal and Al-SBA-15 at 400°C are compared in Table 4.5. Considering the data, biodiesel waste cracking using acidic catalysts lead to increase from 57.50% to 70.10% - 71.10% for %conversion, rise from 11.50% to 12.05% - 13.10% for gaseous product, increase from 46.00% to 57.00% - 59.05% for liquid product and decrease from 42.50% to 28.90% - 29.90% for residue. Although pure SBA-15 is used, the result of catalytic cracking is nearly reached to the activity of acidic catalysts. The obtained liquid yield from acidic catalysts is higher than from pure SBA-15 about 2% - 3% indicating that the acidity of catalyst plays one role on catalytic cracking reaction. However, the values of %conversion and %yield are not significantly different in acidic catalytic reactions when Si/Al ratio increases from 10 to 200. On the other hand, the specific surface area plays an important role on catalytic cracking over mesoporous materials considering on the different conversion between thermal cracking and catalytic cracking. The reason of the comparable activity of acid catalytic cracking is the compromise between the acidity and the specific surface area. In addition, the wall thickness of the catalysts is one considerable parameter for high activity. The reason of this effect might be related to the WBP (pH= 10.47) which contacts directly to catalyst so it is able to destroy hexagonal framework of the catalyst. The hexagonal structure of the used catalyst is demolished by the WBP and this result is

confirmed by XRD pattern as shown in the Figure 4.12. In general for synthesized zeolite or mesoporous materials, it is necessary to dissolve the silica source with alkali solution at the pH of 10 to occur SiO_2 form. In addition, the synthetic materials must be separated from the alkali media after finished crystallization because it can dissolve in base media and transform to the other phases.

Table 4.5 Value of %conversion and %yield obtained by thermal cracking and catalytic cracking of WBP over Al-SBA-15 samples with various Si/Al ratios at 400°C (Condition: 10%wt catalyst of substrate, N_2 flow of 20 mL/min and reaction time of 40 min)

	Thermal	**SBA-15**	**Al-SBA-15(10)**	**Al-SBA-15(25)**	**Al-SBA-15(50)**	**Al-SBA-15(100)**	**Al-SBA-15(200)**
% Conversion*	57.50	68.50	70.60	70.70	70.80	71.10	70.10
% Yield*							
1. Gas fraction	11.50	12.95	12.33	12.60	12.87	12.05	13.10
2. Liquid fraction	46.00	55.55	58.27	58.10	57.93	59.05	57.00
- Distillated liquid	15.47	20.31	20.74	20.62	21.30	20.90	21.43
- Heavy liquid	30.53	35.24	37.53	37.48	36.63	38.15	35.57
3. Residue	42.50	31.50	29.40	29.30	29.20	28.90	29.90
Total volume of liquid fraction (mL)	2.30	2.93	3.05	3.07	3.06	3.09	3.04
Liquid fraction density (g/mL)	1.00	0.95	0.95	0.95	0.95	0.95	0.94

*Deviation within 0.8% for conversion, 0.5% for yield of gas fraction, 0.8% for yield of liquid fraction, and 0.8% for yield of residue.

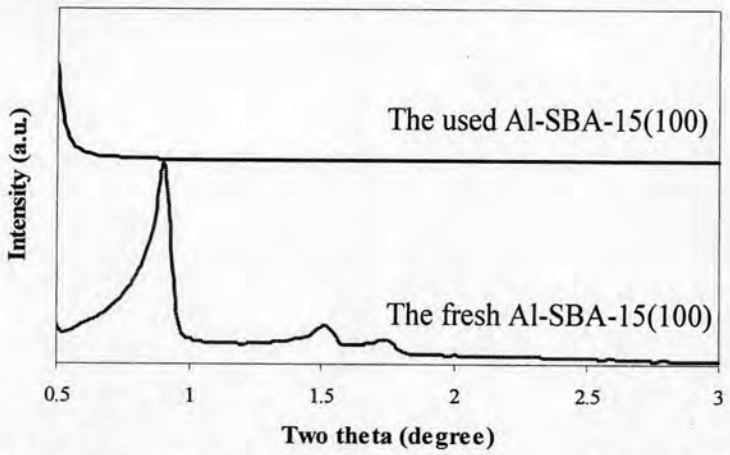

Figure 4.12 XRD patterns of the fresh and the used Al-SBA-15(100) in liquid-phase catalytic cracking.

Figure 4.13 shows distribution of gas fraction obtained by thermal cracking and catalytic cracking of WBP over Al-SBA-15 with various Si/Al ratios at 400°C. In the presence of any mesoporous catalysts, 1,3-butadiene and CO_2 are the predominant gas products. For thermal cracking, the product distribution in gas fraction is similar to catalytic cracking reactions.

Figure 4.14 illustrates distribution of distillated liquid fraction obtained by thermal cracking and catalytic cracking of WBP over Al-SBA-15 with various Si/Al ratios at 400°C. Both thermal cracking and catalytic cracking produce 2-cyclopenten-1-one as the major liquid product. It might be produced from dicarboxylic acid, in which the two carboxyl groups are separated by 4 or 5 carbon atoms on heating alone or distilling with acetic anhydride gave cyclic ketone, for example adipic acid [71].

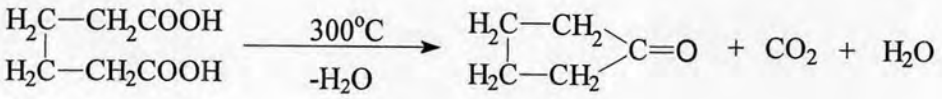

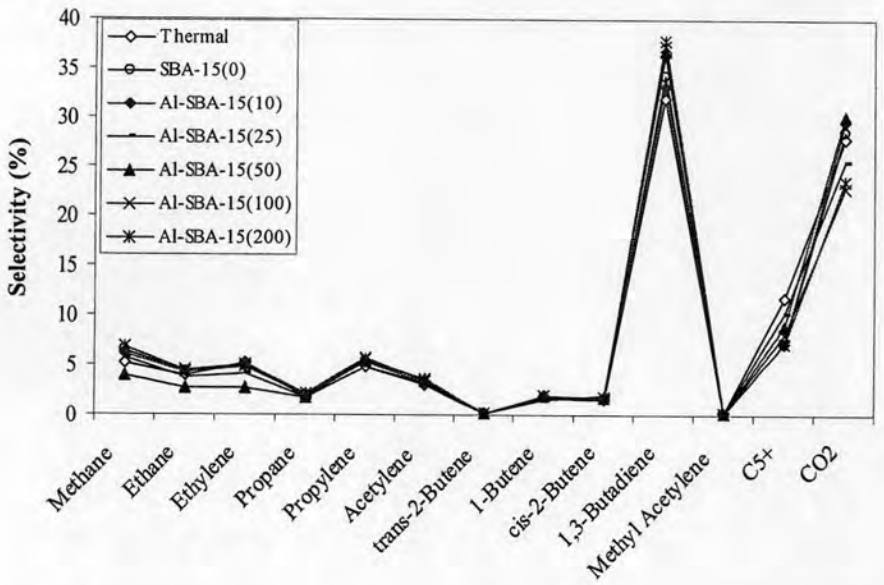

Figure 4.13 Distribution of gas fraction obtained by thermal cracking and catalytic cracking of WBP over Al-SBA-15 samples with various Si/Al ratios at 400°C (Condition: 10%wt catalyst of substrate, N_2 flow of 20 mL/min and reaction time of 40 min).

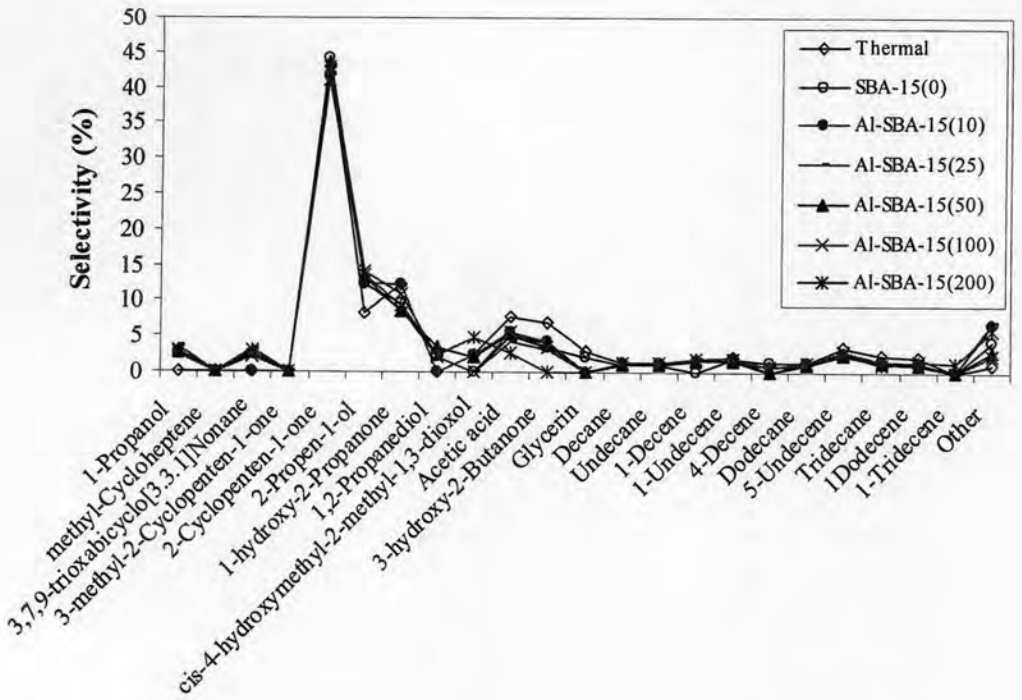

Figure 4.14 Distribution of liquid fraction obtained by thermal cracking and catalytic cracking of WBP over Al-SBA-15 samples with various Si/Al ratios at 400°C (Condition: 10%wt catalyst of substrate, N_2 flow of 20 mL/min and reaction time of 40 min).

According to the results of Si/Al ratio in catalyst effect on WBP cracking, %conversion and %yield perform no significant difference when Si/Al ratio increases from 10 to 200. The values of %conversion are in the range of 70% - 71%, whereas %yields of liquid are observed in the range of 57% - 59%. Then, Al-SBA-15 with Si/Al of 100 is used for further investigation.

4.4.2 Effect of the reaction temperatures

The Al-SBA-15(100) catalyst was used for studying the effect of the reaction temperature on its activity. The accumulative volume of liquid fractions in the graduated cylinder increased as a function of lapsed time is presented in Figure 4.15. When the reaction temperature is increased, the kinetic rate of liquid fraction at the higher reaction temperature is sharper than at the lower reaction temperature. Addition, the total liquid volume was risen when the reaction temperature was increased. However, the initial rate of liquid fraction formation was not different for each reaction temperature.

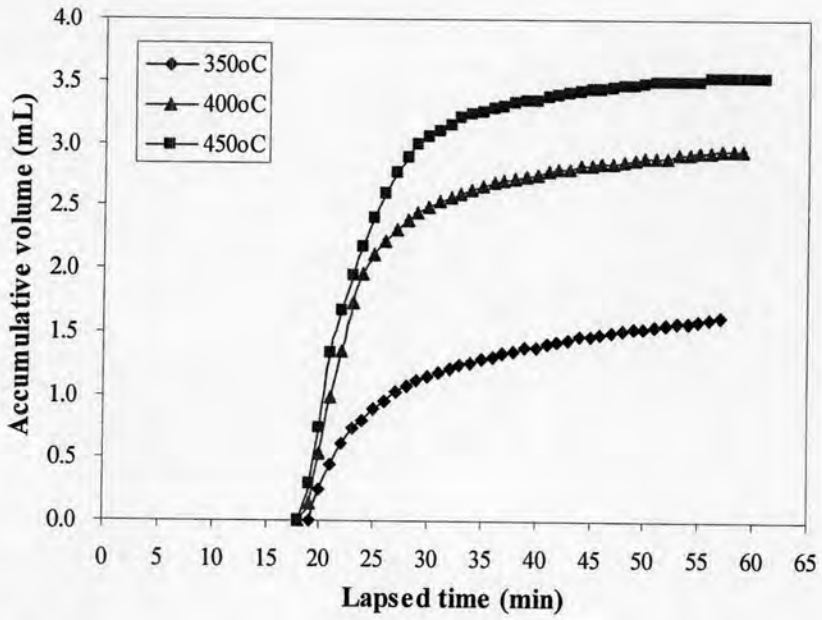

Figure 4.15 Accumulative volume of liquid fraction from catalytic cracking of WBP over Al-SBA-15(100) catalyst at the different reaction temperatures (Condition: 10%wt catalyst of substrate, N_2 flow of 20 mL/min and reaction time of 40 min).

The thermal cracking was tested in comparison. The kinetic rates of thermal cracking exhibited slower than catalytic cracking at the reaction temperature of 400°C and 450°C. The value of %conversion and % yield of the product for thermal cracking and catalytic cracking of WBP over Al-SBA-15(100) catalysts at 350°C, 400°C and 450°C are shown in Table 4.6. When the reaction temperature was increased in catalytic cracking from 350°C to 450°C, the conversion was risen from 41.60% to 83.80%, the gas product was got higher from 7.80% to 16.80%, the liquid fraction was grew from 33.80% to 67.00%, while the residue was remarkable decreased from 58.40% to 16.20%. However, the distillated liquid fraction at the high reaction temperature in catalytic cracking was drop about 13%. At 350°C, the conversion and the product yield performed no significantly difference between thermal cracking and catalytic cracking, while at higher reaction temperatures (400°C-450°C), catalytic cracking showed more effective than pyrolysis. The catalyst performs high activity at the reaction temperature of 400°C and the catalytic effect is decreased when the reaction temperature is increased. It is able to suggest that cracking activity of biodiesel waste depend on the reaction temperature.

Table 4.6 Value of %conversion and %yield obtained by thermal cracking and catalytic cracking of WBP over Al-SBA-15(100) catalyst at the different reaction temperatures (Condition: 10%wt catalyst of substrate, N_2 flow of 20 mL/min and reaction time of 40 min)

	Reaction temperature = 350°C		**Reaction temperature = 400°C**		**Reaction temperature = 450°C**	
	Thermal	**Al-SBA-15(100)**	**Thermal**	**Al-SBA-15(100)**	**Thermal**	**Al-SBA-15(100)**
% Conversion*	40.67	41.60	57.50	71.10	81.00	83.80
% Yield*						
1. Gas fraction	7.73	7.80	11.50	12.05	19.80	16.80
2. Liquid fraction	32.93	33.80	46.00	59.05	61.20	67.00
- Distillated liquid	11.12	15.24	15.47	20.90	18.13	21.45
- Heavy liquid	21.81	18.56	30.53	38.15	43.07	45.55
3. Residue	59.33	58.40	42.50	28.90	19.00	16.20
Total volume of liquid fraction (mL)	1.54	1.75	2.30	3.09	3.20	3.58
Liquid fraction density (g/mL)	1.06	0.97	1.00	0.95	0.96	0.94

*Deviation within 0.8% for conversion, 0.5% for yield of gas fraction, 0.8% for yield of liquid fraction, and 0.8% for yield of residue.

Figure 4.16 shows distribution of gas fraction obtained by thermal cracking and catalytic cracking of WBP over Al-SBA-15(100) sample at 350°C, 400°C and 450°C. All reaction temperature, the major components for both thermal cracking and catalytic cracking are 1,3-butadiene and CO_2. At 350°C, both pyrolysis and catalytic cracking gave CO_2 as the main gas product, while at higher reaction temperatures showed 1,3-butadiene comparable to CO_2. The growing yield of the volatile components with decreasing yield of CO_2 as function of the reaction temperature could be caused by the thermal stability of WBP (glycerol and MONG) might be decreased when the reaction temperature is increased.

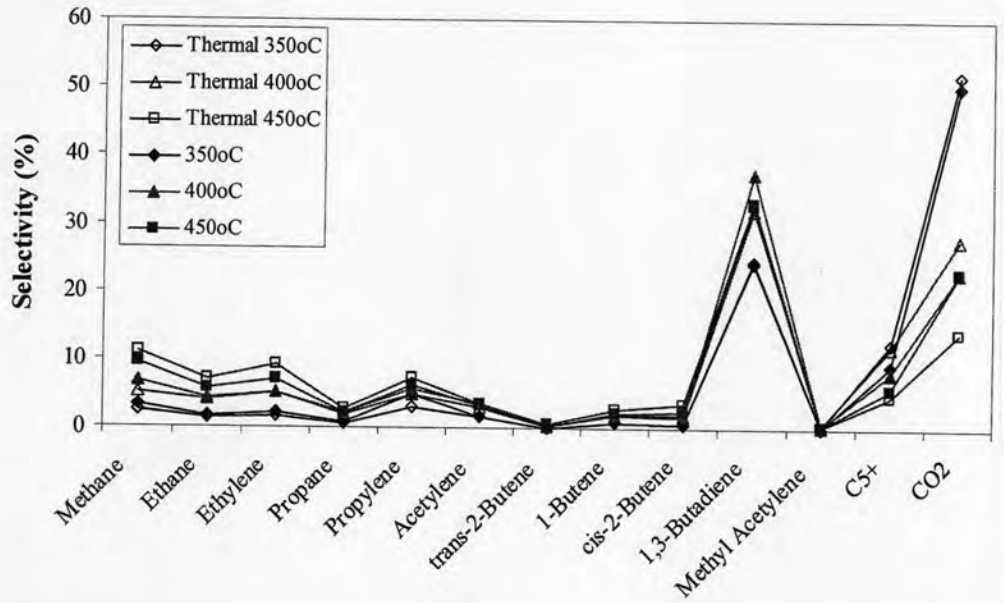

Figure 4.16 Distribution of gas fraction obtained by thermal cracking and catalytic cracking of WBP over Al-SBA-15(100) catalyst at the different reaction temperatures (Condition: 10%wt catalyst of substrate, N_2 flow of 20 mL/min and reaction time of 40 min).

Figure 4.17 exhibits product distribution of distillated liquid fraction obtained by thermal cracking and catalytic cracking of WBP over Al-SBA-15 with various the reaction temperatures. All cracking reactions at various the reaction temperatures produce 2-cyclopenten-1-one as the major liquid product. However, this cyclic ketone was reducing when the reaction temperature was increasing. The absence of 2-cyclopenten-1-one was transformed to hydrocarbon liquid products when the reaction temperature was risen. According to the results of the reaction temperature effect on WBP cracking, the difference between catalytic and non-catalytic reaction was maximum value at the reaction temperature of 400°C. As a result, the reaction temperature of 400°C is selected to be the test condition for further studies in this work.

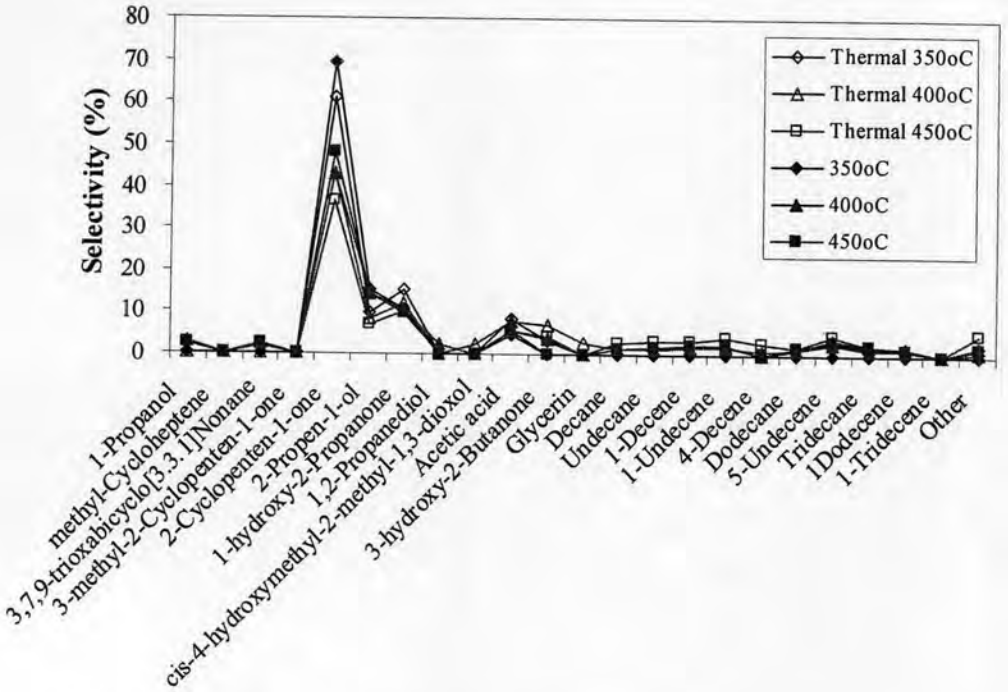

Figure 4.17 Distribution of liquid fraction obtained by thermal cracking and catalytic cracking of WBP over Al-SBA-15(100) catalyst at the different reaction temperatures (Condition: 10%wt catalyst of substrate, N_2 flow of 20 mL/min and reaction time of 40 min).

4.4.3 Effect of waste from biodiesel production to catalyst ratios

Value of %conversion and the product yield obtained by catalytic cracking of WBP at 400°C over Al-SBA-15(100) catalyst with the different catalyst amounts of 2.5%, 5.0%, 10.0% and 15.0% to WBP are shown in Table 4.7. The highest value of 71.10% conversion is obtained when using 10%wt catalyst amount. Reducing of catalyst amounts to 2.5% and 5.0% leads the decreasing value of %conversion to 63.80% and 66.30%, respectively. It indicates that the conversion depends on the catalyst content. However, the %conversion at 15.0wt% catalyst amount does not increase because of the agglomeration of acidic catalyst. Considering to %product yield, the gas fraction yield was slightly increased when the catalyst amount was risen. Basically, the less amount of catalyst which performed low acidity, effected to low conversion of gas and liquid products. The amount of residue and the conversion are inversely related. The residue produced by using the less amount of catalyst is larger than higher catalyst contents.

The selectivity to light and heavy liquid fractions is affected by the catalyst content. The WBP cracking using minimum of catalyst provides low selectivity to distillated liquid fraction because of the less acidity. From the results that mention above, the optimum catalyst amount is the 10.0wt% catalyst to WBP due to providing the greatest %conversion and the highest liquid fraction.

Table 4.7 Value of %conversion and %yield obtained by catalytic cracking of WBP over Al-SBA-15 (100) catalyst with the different catalyst amounts at 400°C (Condition: N_2 flow of 20 mL/min and reaction time of 40 min)

	Catalyst amounts to WBP			
	2.5wt%	**5.0wt%**	**10.0wt%**	**15.0wt%**
% Conversion*	63.80	66.30	71.10	70.00
% Yield*				
1. Gas fraction	11.50	11.70	12.05	12.50
2. Liquid fraction	52.30	54.60	59.05	57.50
- Distillated liquid	17.26	19.95	20.90	22.94
- Heavy liquid	35.04	34.65	38.15	34.56
3. Residue	36.20	33.70	28.90	30.00
Total volume of liquid fraction (mL)	2.73	2.85	3.09	3.00
Liquid fraction density (g/mL)	0.95	0.96	0.95	0.96

*Deviation within 0.8% for conversion, 0.4% for yield of gas fraction, 0.5% for yield of liquid fraction, and 0.8% for yield of residue.

Figure 4.18 shows the accumulative volume of liquid fraction obtained by catalytic cracking of WBP over Al-SBA-15(100) catalyst with different catalyst amounts at 400°C. Although the minimal catalyst amount is utilized, the kinetic rate of liquid fraction performs no significant difference. Upon prolongation of reaction using the 10wt% catalyst amount, the slope is higher than other catalyst amounts, indicating the predominant competitive rate of dissociation of liquid molecules to gas molecules compares to the rate of liquid formation. Although the initial rates of liquid fraction in each conditions show no significant difference, the total liquid volume is depended on the catalyst amount. The liquid yield of catalyst amount of 15.0wt% to WBP performs rarely the same level as the catalyst amount of 10.0 wt %.

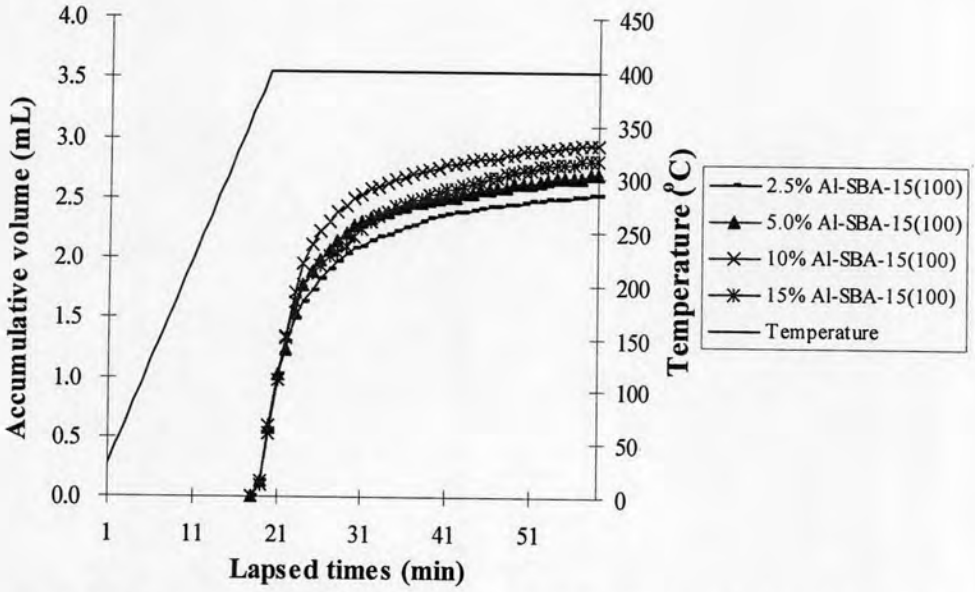

Figure 4.18 Accumulative volume of liquid fraction from catalytic cracking of WBP over Al-SBA-15(100) catalyst with the different catalyst amounts at 400°C (Condition: N_2 flow of 20 mL/min and reaction time of 40 min).

Distribution plots of gas fraction obtained by catalytic cracking of WBP over Al-SBA-15(100) with various catalyst amounts at 400°C are showed in Figure 4.19. The main gases from WBP cracking are 1,3-butadiene and CO_2. The product distribution in gaseous phase for all catalyst amounts is similar.

The product distributions of volatile liquid fraction obtained by catalytic cracking of WBP over Al-SBA-15(100) catalyst with various catalyst amounts at 400°C are demonstrated in Figure 4.20. The product distribution in liquid phase for all catalyst amounts is the same. 2-Cyclopenten-1-one is the major product. In this work, using 10% catalyst amount is the best condition according to the greatest %conversion and the highest liquid fraction.

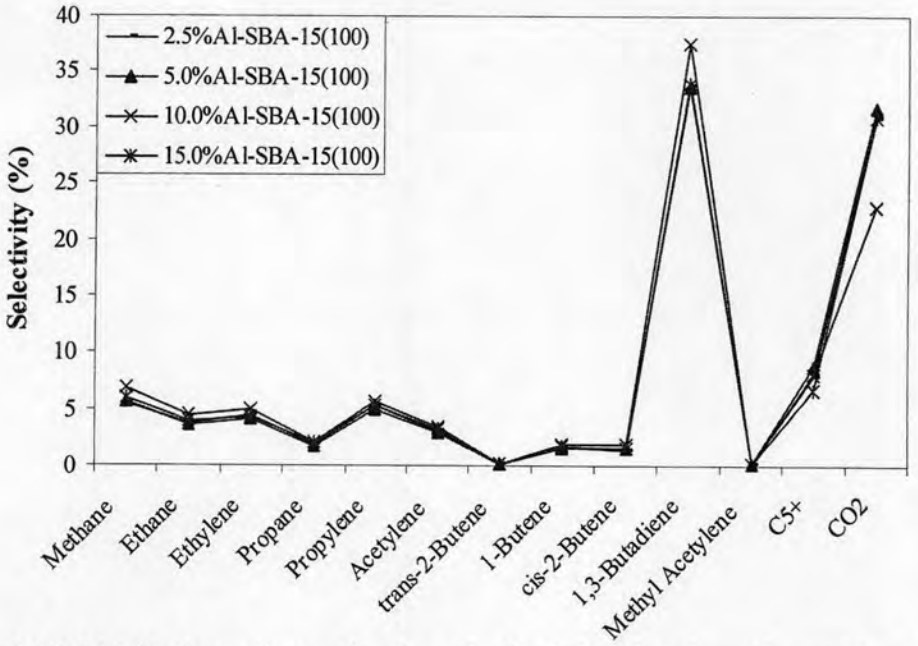

Figure 4.19 Distribution of gas fraction obtained by the thermal cracking and catalytic cracking of WBP over Al-SBA-15(100) catalyst with the different catalyst amounts at 400°C (Condition: N_2 flow of 20 mL/min and reaction time of 40 min).

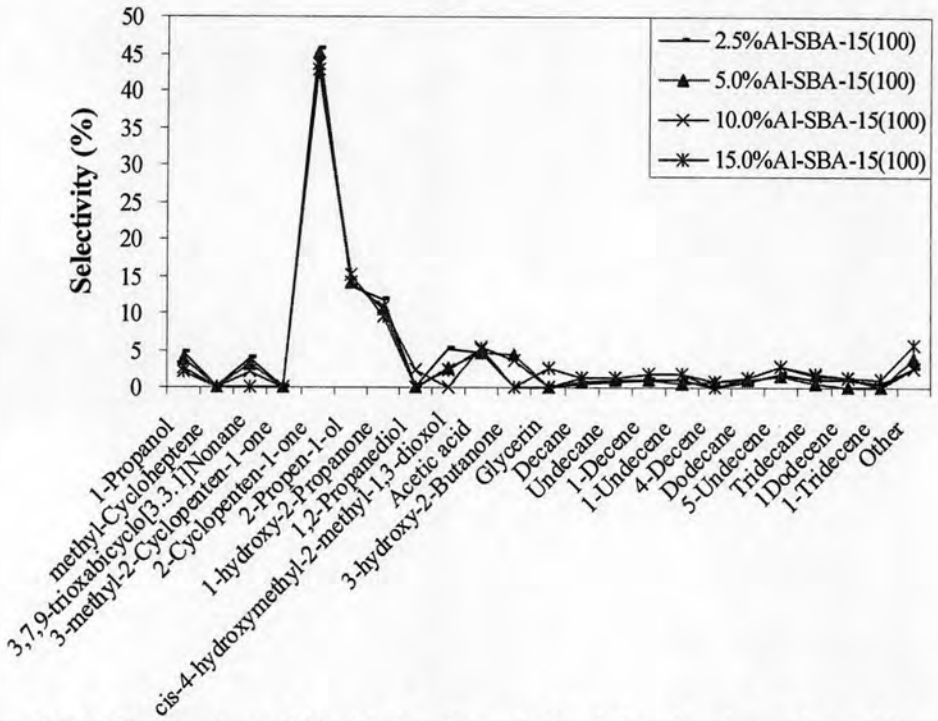

Figure 4.20 Distribution of liquid fraction obtained by the thermal cracking and catalytic cracking of WBP over Al-SBA-15(100) catalyst with the different catalyst amounts at 400°C (Condition: N_2 flow of 20 mL/min and reaction time of 40 min).

4.4.4 Effect of vapour-phase catalytic cracking

Modified silica framework, Al-SBA-15 catalysts cannot be regenerated in catalytic cracking of WBP testing in liquid-phase catalytic reaction because the WBP contacts directly to the catalyst. The vapour-phase catalytic reaction was investigated in this reaction for recycle the catalyst and reduction the cost.

Table 4.8 exhibits %conversion and %yield obtained by thermal cracking and catalytic cracking of WBP over fresh Al-SBA-15(100) at 400°C in vapour-phase catalytic cracking and liquid-phase catalytic reaction. For pyrolysis, thermal-VAP exhibits higher conversion value than thermal-LIQ because of the sieve. Although the sieve increases the activity of liquid fraction about 2%, the light liquid fraction drops about 5%. Considering on catalytic cracking, the %conversion of catalytic-LIQ is higher 14% than thermal-LIQ, while catalytic-VAP gives 5% less than thermal-VAP. In addition, catalytic-LIQ produces liquid fraction greater than catalytic-VAP nearly about 20% including the total liquid volume. However, the catalyst in vapour-phase catalytic reaction is able to perform its efficiency to crack the large molecule to smaller ones considering on distillated liquid fraction which gives double times than the others. Moreover, the used catalyst can be regenerated for the next run that is the most important advantage of the heterogeneous catalyst besides the ease of separation from the reaction. According to the result, vapour-phase catalytic reaction exhibits many advantages than liquid-phase catalytic reaction. It is interesting for the further study on vapour-phase reaction to solve the basic-starting material problem.

Table 4.8 Value of %conversion and %yield obtained by thermal cracking and catalytic cracking of WBP over Al-SBA-15(100) at 400°C in vapour-phase catalytic cracking and liquid-phase catalytic cracking (Condition: 10%wt catalyst of substrate, N_2 flow of 20 mL/min and reaction time of 40 min)

	Vapour-phase		Liquid-phase	
	Thermal	**Al-SBA-15(100)**	**Thermal**	**Al-SBA-15(100)**
% Conversion*	59.60	54.40	57.50	71.10
% Yield*				
1. Gas fraction	11.00	14.00	11.50	12.05
2. Liquid fraction	48.60	40.40	46.00	59.05
- Distillated liquid	13.94	27.41	15.47	20.90
- Heavy liquid	34.66	12.99	30.53	38.15
3. Residue	40.40	45.60	42.50	28.90
- wax	-	42.32	-	-
- Solid coke	-	3.28	-	-
Total volume of liquid fraction (mL)	2.43	2.23	2.30	3.09
Liquid fraction density (g/mL)	1.00	0.91	1.00	0.95

*Deviation within 1.0% for conversion, 0.8% for yield of gas fraction, 0.8% for yield of liquid fraction, and 1.0% for yield of residue.

Figure 4.21 shows the accumulative volume of liquid fraction in the graduated cylinder obtained by thermal cracking and catalytic cracking of WBP over Al-SBA-15(100) at 400°C in vapour-phase catalytic cracking and liquid-phase catalytic cracking. The kinetic rate of liquid fraction formation over catalytic-LIQ is faster than others. Although Al-SBA-15 was utilized as catalyst in vapour-phase catalytic cracking (catalytic-VAP), the kinetic rate shows no difference comparative with thermal-VAP. However, the initial rate of liquid formation in the pyrolysis of WBP is slower than catalytic reaction indicating the catalytic sieve obstructs the pathway of liquid product at the early reaction.

Distribution of gas fraction obtained by pyrolysis and catalytic cracking of WBP over Al-SBA-15(100) catalyst at 400°C in vapour-phase catalytic cracking and liquid-phase catalytic cracking are showed in Figure 4.22. The volatile gas products obtained

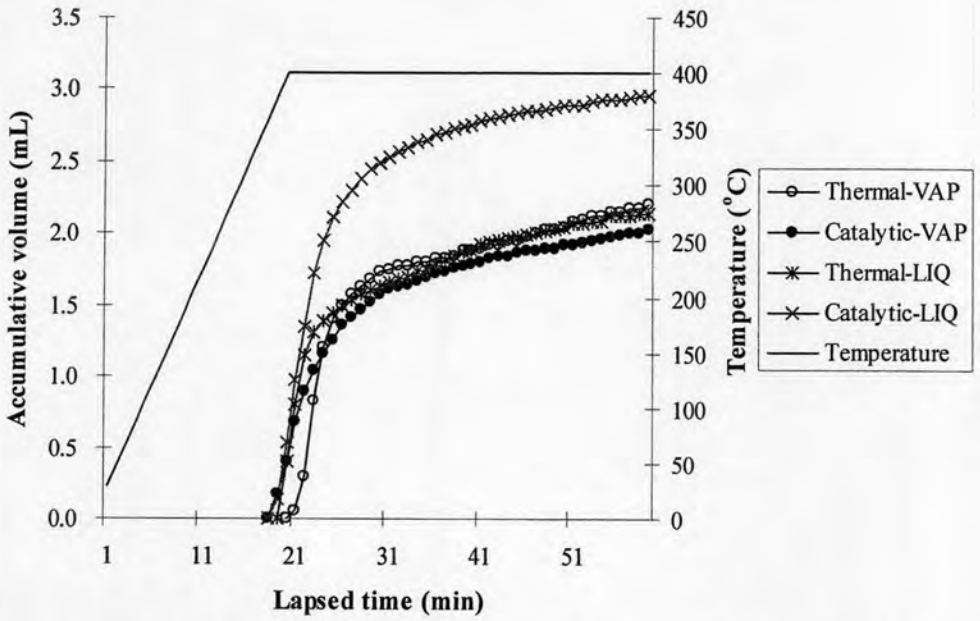

Figure 4.21 Accumulative volume of liquid fraction from thermal cracking and catalytic cracking of WBP over Al-SBA-15(100) at 400°C in vapour-phase catalytic cracking and liquid-phase catalytic cracking (Condition: 10%wt catalyst of substrate, N_2 flow of 20 mL/min and reaction time of 40 min).

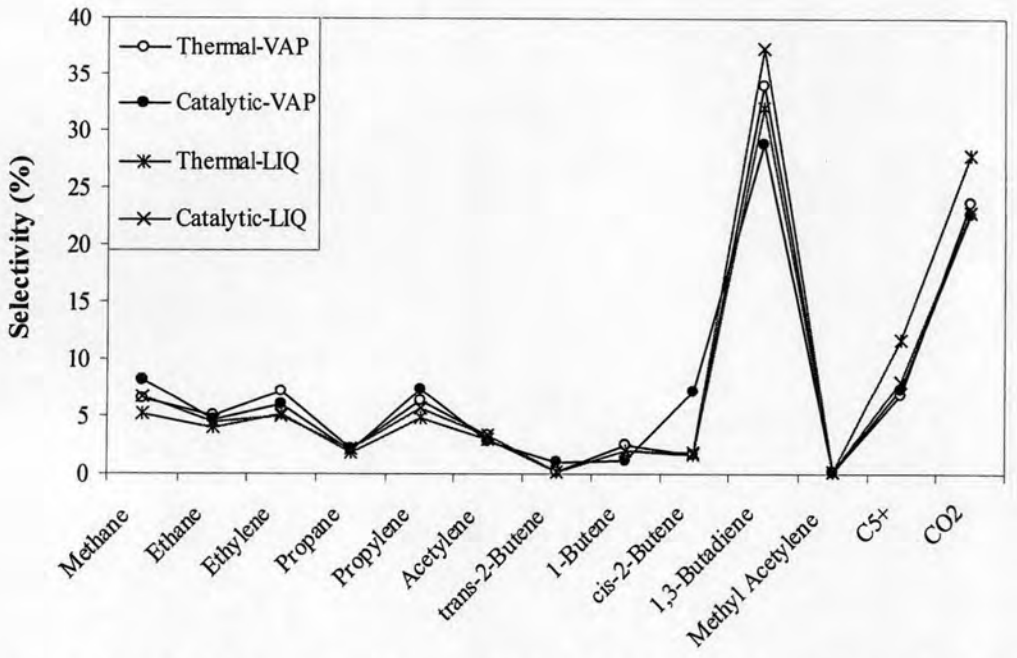

Figure 4.22 Distribution of gas fraction obtained by the thermal cracking and catalytic cracking of WBP over Al-SBA-15(100) at 400°C in vapour-phase catalytic cracking and liquid-phase catalytic cracking (Condition: 10%wt catalyst of substrate, N_2 flow of 20 mL/min and reaction time of 40 min).

by vapour-phase catalytic reaction are larger than received from liquid-phase catalytic reaction. In addition,cis-2-butene is produced by catalytic-VAP, while found minimum from others condition. The main gases from WBP cracking are 1,3-butadiene and CO_2 which catalytic-LIQ provides the highest quantity of 1,3-butadiene. It seems vapour-phase and liquid-phase catalytic reaction performing no significant difference in the selectivity of gas products.

Considering the distribution of volatile liquid fraction obtained by the thermal cracking and catalytic cracking of WBP over Al-SBA-15(100) catalyst 400°C in vapour-phase catalytic cracking and liquid-phase catalytic cracking are showed in Figure 4.23. The volatile liquid products can be classified into two groups, vapour-phase and liquid-phase. For vapour-phase, the main volatile liquid products are methyl-cycloheptene, 3-methyl-2-cyclopenten-1-one, 2-cyclopenten-1-one, and 2-propen-1-ol, while 2-cyclopenten-1-one, 2-propen-1-ol, acetic acid, and 3-hydroxy-2-butanone are the major products in liquid-phase. However, the first main product for all reactions is 2-cyclopenten-1-one. In view of vapour-phase reaction, pyrolysis favors to produce 2-propen-1-ol as the second major liquid product, whereas catalytic prefers to generate 3-methyl-2-cyclopenten-1-one instead.

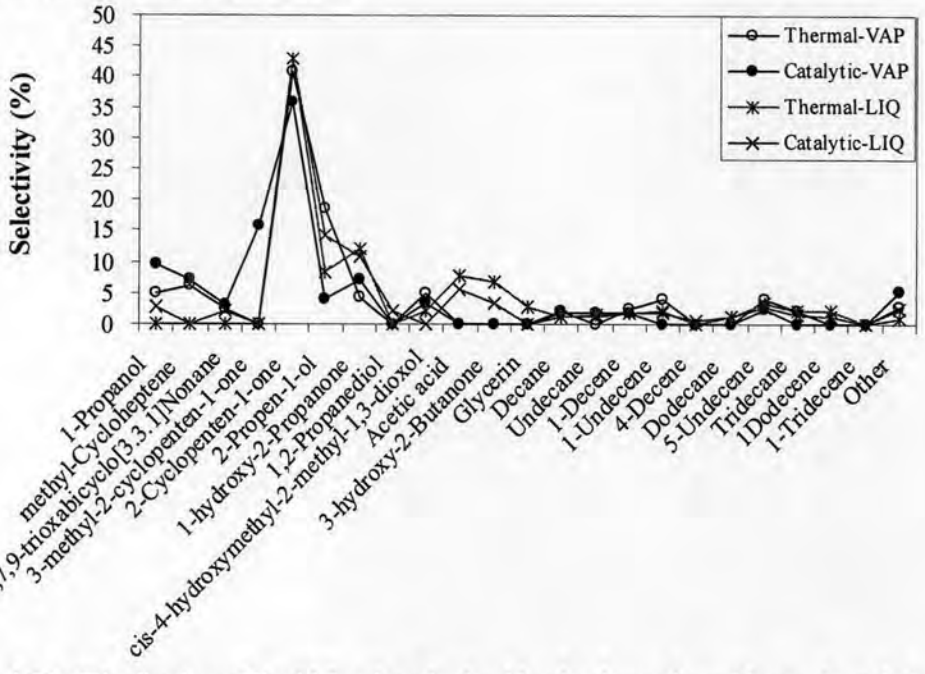

Figure 4.23 Distribution of liquid fraction obtained by the thermal cracking and catalytic cracking of WBP over Al-SBA-15(100) at 400°C in vapour-phase catalytic cracking and liquid-phase catalytic cracking (Condition: 10%wt catalyst of substrate, N_2 flow of 20 mL/min and reaction time of 40 min).

4.5 Catalyst regenerations

The studied condition was 10%wt catalyst of substrate, N_2 flow of 20 mL/min and reaction time of 40 min at 400°C using Al-SBA-15(100). Characterization of regenerated catalysts is necessary for explanation in the activity of recycle reactions.

4.5.1 Characterization of the regenerated catalysts

4.5.1.1 XRD results of the regenerated catalysts

After the reaction was complete, the surface and pores of Al-SBA-15(100) catalyst are deposited with the coke produced in the reaction. In this research, the used catalyst is washed with hexane to remove wax for several times, and dried at 100°C. Before the next run, it must be calcined at 550°C for 5 h and denoted as the 1st regenerated. In addition, the 1st regenerated was used in catalytic cracking of WBP and treated for the next testing similar as the fresh catalyst, coded as the 2nd regenerated. Figure 4.24 shows XRD patterns of the fresh and the regenerated catalysts of the 1st and the 2nd cycles in vapour-phase. The XRD patterns of regenerated catalysts are a typical XRD pattern of hexagon like fresh Al-SBA-15 catalyst. However, they were shifted slightly to higher angle than fresh catalyst indicating the shrinkage during the calcination processes.

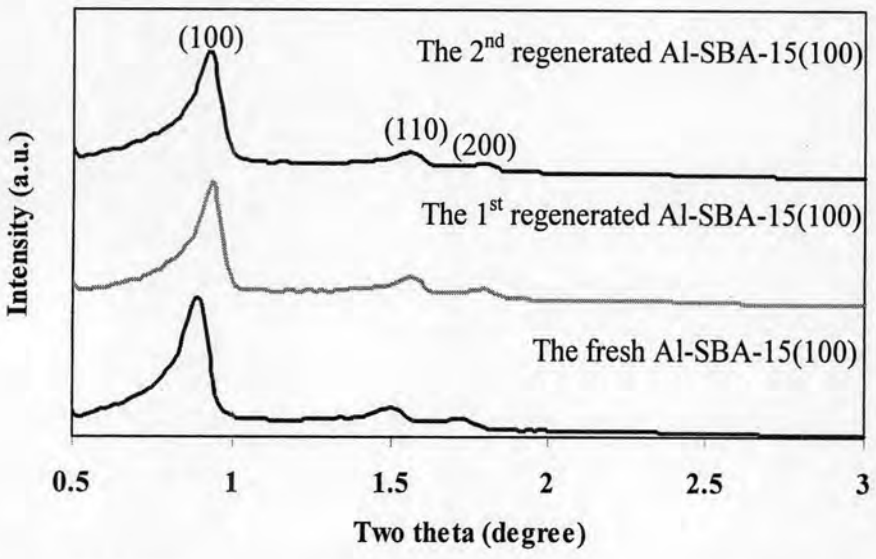

Figure 4.24 XRD patterns of the fresh and the regenerated Al-SBA-15(100) in vapour-phase catalytic cracking.

4.5.1.2 Sorption properties of the regenerated catalysts

The adsorption-desoprtion isotherms of the fresh and the regenerated catalysts are shown in Figure 4.25. The regenerated catalysts display the characteristic isotherm type IV with H1-type hysteresis loop of mesoporous materials. Textural properties of fresh Al-SBA-15 and regenerated catalysts are concluded in Table 4.9. The specific surface area is slightly reduced by 13% for the 1st regenerated catalyst and 17% for the 2nd regenerated catalyst as compared to the fresh one.

Table 4.9 Textural properties of the fresh and the regenerated Al-SBA-15(100) catalysts

Sample	Total specific surface area[a] ($m^2 \cdot g^{-1}$)	Pore size distribution[b] (nm)	Mesopore volume[b] ($cm^3 \cdot g^{-1}$)	$d_{(100)}$[c] (nm)	Wall thickness[d] (nm)
Fresh	703	9.23	1.132	9.56	1.81
1st regenerated	610	9.23	1.039	9.53	1.77
2nd regenerated	582	9.23	1.029	9.59	1.84

[a]Calculated using the BET plot method,

[b]Calculated using the BJH method,

[c]Calculated using XRD, Jade5.6,

[d]Calculated as: a_0-pore size ($a_0 = 2 \times d_{(100)} / \sqrt{3}$).

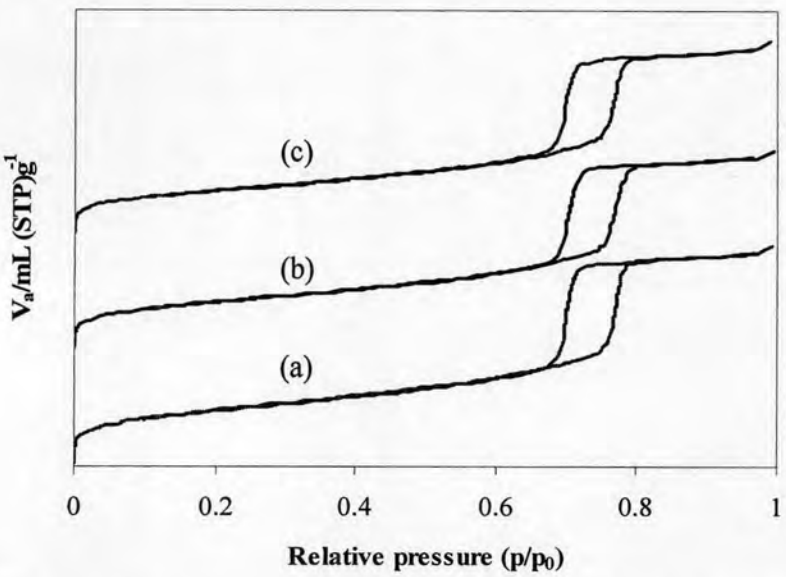

Figure 4.25 N_2 adsorption-desorption isotherms of (a) the fresh, (b) the 1st regenerated and (c) the 2nd regenerated Al-SBA-15(100) catalysts.

4.5.2 Activity of regenerated Al-SBA-15(100) on WBP cracking

The value of %conversion and % yield of products obtained by catalytic cracking of WBP at 400°C over the fresh, the 1st regenerated and the 2nd regenerated of Al-SBA-15(100) in vapour-phase catalytic cracking are shown in Table 4.10. The thermal cracking was test in comparison. Although the total liquid volume of pyrolysis is higher than catalytic cracking, the distillated liquid fraction of catalytic cracking is higher than the thermal cracking about 2.5 times. Considering on catalytic cracking, the values of %conversion, yield of product including total liquid volume over the 1st regenerated catalyst are the same as the results over fresh catalyst. While the 2nd regenerated catalyst exhibits lower conversion and liquid fraction than the fresh and the 1st regenerated catalyst. However, yield of gas fraction and the distillated liquid fraction are not significantly different from the fresh one. This result may be a cause the 2nd regenerated has a lower surface area and acidity comparative to the fresh and the 1st regenerated catalyst.

Figure 4.26 show the accumulative volume of liquid fraction in the graduated cylinder obtained by thermal cracking and catalytic cracking of WBP over the fresh, the 1st regenerated and the 2nd regenerated Al-SBA-15(100) catalyst 400°C in vapour-phase catalytic cracking. The initial rate of liquid fraction formation over the fresh and the 1st regenerated catalyst are faster than the 2nd regenerated catalyst. Although the initial rate of liquid formation in the pyrolysis of WBP is slower than the catalytic reaction, the propagation of kinetic rate and the total liquid volume is higher than the catalytic cracking.

Table 4.10 Value of %conversion and %yield obtained by thermal cracking and catalytic cracking of WBP over the fresh, the 1st regenerated and the 2nd regenerated Al-SBA-15(100) catalysts at 400°C in vapour-phase catalytic cracking (Condition: 10%wt catalyst of substrate, N_2 flow of 20 mL/min and reaction time of 40 min)

	Al-SBA-15(100)			
	Thermal	**Fresh**	**1st regenerated**	**2nd regenerated**
% Conversion*	59.60	54.40	55.60	51.00
% Yield*				
1. Gas fraction	11.00	14.00	15.00	14.80
2. Liquid fraction	48.60	40.40	40.60	36.20
- Distillated liquid	13.94	27.41	28.48	23.92
- Heavy liquid	34.66	12.99	12.12	12.28
3. Residue	40.40	45.60	44.40	49.00
- Wax	-	42.32	41.15	46.01
- Solid coke	-	3.28	3.25	2.99
Total volume of liquid fraction (mL)	2.43	2.23	2.27	2.00
Liquid fraction density (g/mL)	1.00	0.91	0.90	0.91

*Deviation within 1.0% for conversion, 0.8% for yield of gas fraction, 0.8% for yield of liquid fraction, and 1.0% for yield of residue.

Distribution of gas fraction obtained by the WBP cracking using the fresh and regenerated Al-SBA-15(100) catalysts at 400°C is illustrated in Figure 4.26. The gas fraction composes the same product distribution. There are no differences in the selectivity in gas fraction between thermal cracking and catalytic cracking. The major gas products are 1,3-butadiene and CO_2. However, thermal cracking provides smaller cis-2-butene than acid catalytic cracking.

Product distributions of liquid fraction obtained by WBP cracking using fresh and regenerated catalysts are shown in Figure 4.27. Both pyrolysis and catalytic cracking provide 2-cyclopenten-1-one as mainly product in liquid fraction. However, the second product of catalytic cracking is 3-methy-2-cyclopenten-1-one, derivative of major product, whereas 2-propen-1-ol is produced from pyrolysis as the

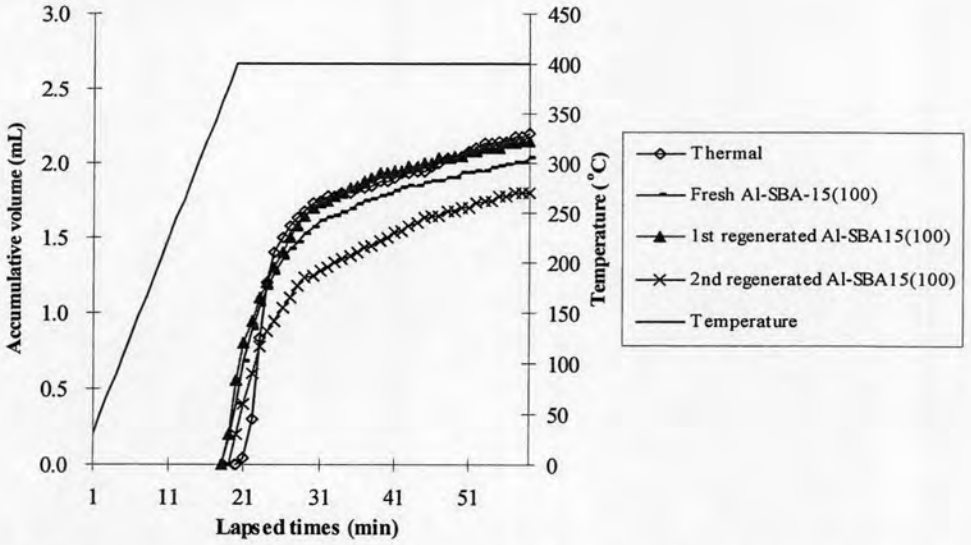

Figure 4.26 Accumulative volume of liquid fraction from thermal cracking and catalytic cracking of WBP over the fresh, the 1st regenerated and the 2nd regenerated Al-SBA-15(100) catalysts at 400°C in vapour-phase catalytic cracking (Condition: 10%wt catalyst of substrate, N_2 flow of 20 mL/min and reaction time of 40 min).

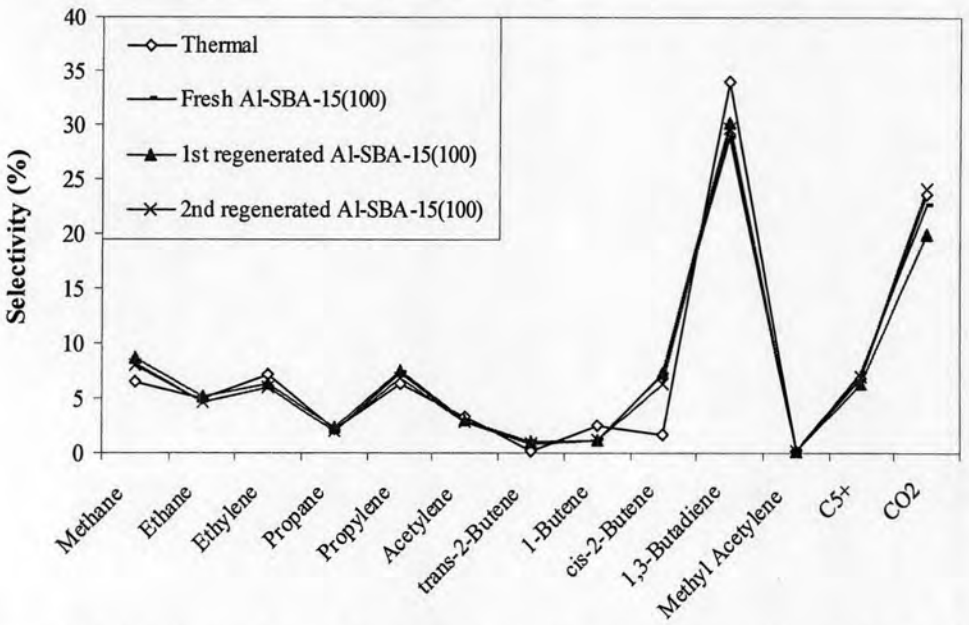

Figure 4.27 Distribution of gas fraction obtained by thermal cracking and catalytic cracking of WBP over the fresh, the 1st regenerated and the 2nd regenerated Al-SBA-15(100) catalysts at 400°C in vapour-phase catalytic cracking (Condition: 10%wt catalyst of substrate, N_2 flow of 20 mL/min and reaction time of 40 min).

second product. The product selectivity of regenerated catalysts does not different from fresh catalyst. The total liquid volume is about the same for fresh and the 1st regenerated catalyst which slightly higher than 2nd regenerated catalyst.

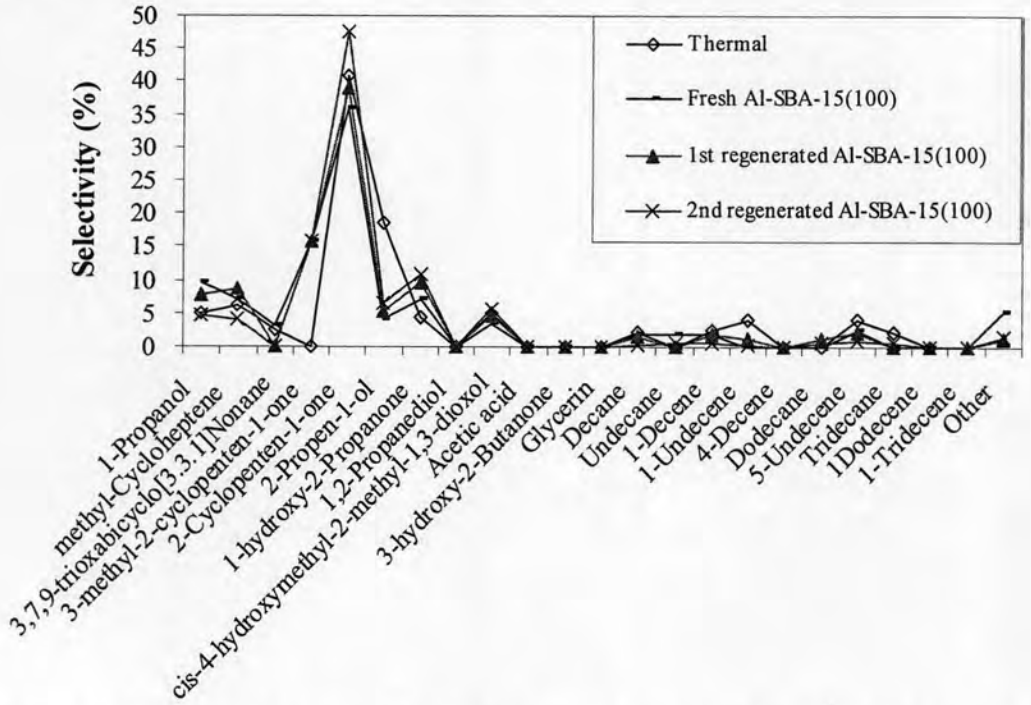

Figure 4.28 Distribution of liquid fraction obtained by thermal cracking and catalytic cracking of WBP over the fresh, the 1st regenerated and the 2nd regenerated Al-SBA-15(100) catalysts at 400°C in vapour-phase catalytic cracking (Condition: 10%wt catalyst of substrate, N_2 flow of 20 mL/min and reaction time of 40 min).

As a result, Al-SBA-15(100) is stable for use as cracking catalyst and the used catalyst can be regenerated easily. The cracking activity shows no significant difference for the first regenerated cycle and a few changes to 3% lower conversion for the second regenerated cycle comparable with the fresh catalyst.